# Polarization gating and circularly-polarized high harmonic generation using plasmonic enhancement in metal nanostructures

**A. Husakou,**[1,*] **F. Kelkensberg,**[2] **J. Herrmann,**[1] **and M. J. J. Vrakking**[1,2]

[1]*Max Born Institute for Nonlinear Optics and Short Pulse Spectroscopy Max Born Str. 2a, D-12489 Berlin, Germany*
[2]*FOM Institute AMOLF, Science Park 104, 1098 XG Amsterdam, The Netherlands*
[*]*gusakov@mbi-berlin.de*

**Abstract:** We investigate possibilities to utilize field enhancement by specifically designed metal nanostructures for the generation of single attosecond pulses using the polarization gating technique. We predict the generation of isolated 59-attosecond-long pulses using 15-fs pump pulses with only a 0.6 TW/cm$^2$ intensity. Our simulations also indicate the possibility to generate previously inaccessible high- harmonics with circular polarization by using an ensemble of vertically and horizontally orientated bow-tie structures. In the numerical simulation we used an extended Lewenstein model, which includes the spatial inhomogeneity in the hot spots and collisions of electrons with the metal surface.



**OCIS codes:** (190.2620) Harmonic generation and mixing; (350.4238) Nanophotonics and photonic crystals.

## References and links

1. M. Hentschel, R. Kienberger, C. Spielmann, G. A. Reider, N. Milosevic, T. Brabec, P. Corkum, U. Heinzmann, M. Drescher, and F. Krausz, "Attosecond metrology," Nature **414**, 509–513 (2001).
2. A. Paul, R. A. Bartels, R. Tobey, H. Green, S. Weiman, I. P. Christov, M. M. Murnane, H. C. Kapteyn, and S. Backus, "Quasi phase matched generation of coherent extreme ultraviolet light," Nature **421**, 51–54 (2003).
3. X. Zhang, A. L. Lytle, T. Popmintchev, X. Zhou, H. C. Kapteyn, M. M. Murnane, and O. Cohen, "Quasi-phase-matching and quantum path control of high-harmonic generation using counterpropagating light," Nat. Phys. **3**, 270–275 (2007).
4. P. B. Corkum and F. Krausz, "Attosecond science," Nat. Phys. **3**, 381–387 (2007).
5. H. Kapteyn, O. Cohen, I. Christov, and M. Murnane, "Harnessing attosecond science in the quest for coherent X-rays," Science **317**, 775–778 (2007).
6. M. F. Kling and M. J. Vrakking, "Attosecond electron dynamics," Annu. Rev. Phys. Chem. **59**, 463–492 (2008).
7. F. Krausz and M. Ivanov, "Attosecond physics," Rev. Mod. Phys. **81**, 163–234 (2009).
8. G. Sansone G. Sansone, F. Kelkensberg, J. F. Perez-Torres, F. Morales, M. F. Kling, W. Siu, O. Ghafur, P. Johnsson, M. Swoboda, E. Benedetti, F. Ferrari, F. Lepine, J. L. Sanz-Vicario, S. Zherebtsov, I. Znakovskaya, A. L.Huillier, M. Yu. Ivanov, M. Nisoli, F. Martin, and M. J. J. Vrakking, "Electron localization following attosecond molecular photoionization," Nature **465**, 763–766 (2010).
9. P. B. Corkum, N. H. Burnett, and M. Y. Ivanov, "Subfemtosecod pulses," Opt. Lett. **19**, 1870–1872 (1994).
10. O. Tcherbakoff, E. Mevel, D. Descamps, J. Plumridge, and E. Constant , "Time gated high order harmonic generation," Phys. Rev. A **68**, 043804 (2003).
11. M. Kovacev, Y. Mairesse, E. Priori, H. Merdji, O. Tcherbakoff, P. Monchicourt, P. Breger, E. Mevel, E. Constant, P. Salieres, B. Carre, and P. Agostini, "Temporal confinement of the harmonic emission through polarization gating," Eur. Phys. J. D **26**, 79–82 (2003).

#156477 - $15.00 USD Received 17 Oct 2011; revised 15 Nov 2011; accepted 15 Nov 2011; published 28 Nov 2011

12. D. Oron, Y. Silberberg, N. Dudovich, and D. M. Villeneuve, "Efficient polarization gating of high-order harmonic generation by polarization-shaped ultrashort pulses," Phys. Rev. A **72**, 063816 (2006).
13. I. J. Sola, E. Mevel, L. Elouga, E. Constant, V. Strelkov, L. Poletto, P. Villoresi, E. Benedetti, J.-P. Caumes, S. Stagira, C. Vozzi, G. Sansone, and M. Nisoli, "Controlling attosecond electron dynamics by phase-stabilized polarization gating", Nat. Phys. **2**, 319–322 (2006).
14. S. Kim, J. Jin, Y.-J. Kim, I.-Y. Park, Y. Kim, and S.-W. Kim, "High-harmonic generation by resonant plasmon field enhancement," Nature **453**, 757–760 (2008).
15. I.-Y. Park, S. Kim, J. Choi, D.-H. Lee, Y.-J. Kim, M. F. Kling, M. I. Stockman, and S.-W. Kim, "Plasmonic generation of ultrashort extreme-ultraviolet light pulses," Nat. Photon. **5**, 677-681 (2011).
16. A. Husakou, S.-J. Im, and J. Herrmann, "Theory of plasmon-enhanced high-harmonic generation in the vicinity of metal nanostructures in noble gases," Phys. Rev. A. **83**, 043839 (2011).
17. S. L. Stebbings, F. Süßmann, Y.-Y. Yang, A. Scrinzi, M. Durach, A. Rusina, M. I. Stockman, and M. F. Kling, "Generation of isolated attosecond extreme ultraviolet pulses employing nanoplasmonic field enhancement: optimization of coupled ellipsoids," New J. Phys. **13**, 073010 (2011).
18. M. Lewenstein, Ph. Balcou, M. Yu. Ivanov, Anne L.Huillier, and P. B. Corkum, "Theory of high-harmonic generation by low-frequency laser fields," Phys. Rev. A **49**, 2117–2132 (1994).
19. Gy. Farkas, Cs. Toth, S. D. Moustaizis, N. A. Papadogiannis, and C. Fotakis, "Observation of multiple-harmonic radiation induced from a gold surface by picosecond neodymium-doped yttrium aluminum garnet laser pulses," Phys. Rev. A **46**, R3605 (1992).
20. P. Biagioni, J. S. Huang, L. Duo, M.Finazzi, and B. Hecht, "Cross resonant optical antenna," Phys. Rev. Lett. **102**, 256801 (2009).
21. G. Sansone, E. Benedetti, F. Calegari, C. Vozzi, L. Avaldi, R. Flammini, L. Poletto, P. Villoresi, C. Altucci, R. Velotta, S. Stagira, S. De Silvestri and M. Nisoli, "Isolated single-cycle attosecond pulses," Science **314**, 443–446 (2006).

---

High harmonic generation (HHG) by intense femtosecond pulses in noble gases has been comprehensively investigated for many years. It is used as the basis for compact table-top sources of coherent soft X-ray radiation and attosecond pulses [1–8]. These sources find applications in a wide range of fields, e.g. attosecond pulses are used in time-resolved studies of electron dynamics on their natural time-scale. For this purpose it is often preferable to have an isolated attosecond pulse, rather than an attosecond pulse train. Such isolated attosecond pulse sources rely on techniques in which HHG emission is restricted to a single half-cycle of the femtosecond driver laser pulse. This condition can be met by using a linearly polarized driving pulse with a duration of only a few optical cycles [1] or by using the polarization gating techniques in which the driver pulse displays a time-varying polarization, which becomes linear only for a short time [9–13]. Due to the high required intensities – larger than 10 TW/cm$^2$ – the generation of high-order harmonics relies on femtosecond laser amplifiers with typical repetition rates in the range of a few kHz. At present many groups follow different approaches with the aim to increase the repetition rate of HHG sources to the MHz range. One of the possibilities to realize this aim is based on the utilization of plasmonic field enhancement by metallic nanostructures. Kim *et al.* [14] have demonstrated that high harmonics can be generated by nanojoule pulses with a repetition rate of 80 MHz (directly from a laser oscillator without amplifiers) by exploiting the local field enhancement of bowtie-shaped gold nanoelements. Later, this approach was extended for the cases of tapered hollow metallic waveguide [15]. Recently, a semiclassical model for plasmon-enhanced HHG in the vicinity of metal nanostructures has been developed [16] which includes the important influence of the field inhomogeneity in the hot spots and the metal surface in the HHG process. A theoretical study of plasmon-enhanced HHG by gold ellipsoidal nanoparticles neglecting the field inhomogeneity has also been presented in Ref. [17].

Based on the model of Ref. [16] in the present paper we study a modified design of bowtie-shaped nanostructures which enables the generation of single attosecond pulses by using the polarization gating technique. We show that by using this design isolated attosecond pulses can be generated from 15 fs pump pulses with a 0.12 TW/cm$^2$ intensity. Additionally, we predict that specially designed metal nanostructure arrays enable the previously unattainable generation

#156477 - $15.00 USD Received 17 Oct 2011; revised 15 Nov 2011; accepted 15 Nov 2011; published 28 Nov 2011

of circularly-polarized harmonics from circularly-polarized pumpi laser pulses.

We describe HHG in the framework of an extended Lewenstein model [16]. According to the three-step Lewenstein model, in the first step the strong electric field $\mathbf{E}(t)$ of the driving pulse ionizes an atom at a time $t_s$ and creates a free electron in the continuum. The free electron is accelerated by the oscillating field and for a linearly polarized field is driven back to the parent ion after the field changes its direction. In the last step the recombination with the parent ion at a moment $t_f$ leads to the emission of a high-energy photon. Neglecting the Coulomb potential, one can represent the time-dependent high-harmonic dipole moment in the direction of the field polarization $x$ as [18]

$$\begin{aligned} d(t_f) = i\frac{e}{2\omega_0^{5/2}m_e}\int_{-\infty}^{t_f}\left(\frac{\pi}{\varepsilon+i\Delta t/2}\right)^{3/2} H(t_f,t_s) \\ \times d_x(p_{st}-eA(t_s))\exp(-i\frac{S(t_f,t_s)}{\hbar}) \\ \times d_x^*(p_{st}-eA(t_f))E(t_s)dt_s + c.c. \end{aligned} \quad (1)$$

In this expression the integration is performed over all past ionization moments $t_s$, $d_x(p-eA(t_s))$ is the dipole moment for a transition from the ground state to the continuum with a kinetic momentum $p-eA(t_s)$, $p=m_e v+eA$ is the canonical momentum, $A(t)$ is the vector potential with $\dot{A}\equiv dA(t)/dt=E(t)$, $S(t_f,t_s)=S_0(t_f,t_s)=I_p\Delta t-0.5e^2(\Delta B^2/\Delta t+\Delta C)/m_e$ is the classical action of an electron in the field, where $\dot{C}(t)=A^2(t)$ and $I_p$ is the ionization potential. The canonical momentum $p_{st}$ is given by $p_{st}=e\Delta B/\Delta t$ with $\dot{B}(t)=A(t)$, $\Delta t\equiv t_f-t_s$, $\varepsilon$ is an arbitrary small regularization parameter, $\omega_0$ is the central laser frequency and $m_e$ the electron mass. For any function $F$ we define $\Delta F\equiv F(t_f)-F(t_s)$. For the ground state of a hydrogenlike atom the dipole matrix element is $d_x(p)=i2^{7.25}[\hbar\omega_0 m_e^2 I_p]^{5/4}\pi^{-1}p/(p^2+\alpha)^3$, where $\alpha=2m_e^{1/2}I_p^{1/2}$. In the unmodified Lewenstein model we have $H(t_f,t_s)\equiv 1$; in the modified case it can take other values as discussed below.

The semiclassical HHG model has been extended [16] to account for the inhomogeneity of the field in the hot spot by writing $E(t,x)=E(t)(1+x/d_{inh})$, In other words, a linear spatial variation of the electric field strength along the diretion of the polarization is included, which is described by a scaling parameter $d_{inh}$. Considering this derivative term as a perturbation, we get a correction $x^{(1)}(t)=-e/(d_{inh}m_e)\int_{t_s}^{t}dt'\int_{t_s}^{t'}E(t'')x^{(0)}(t'')dt''$ to the zeroth-order electron trajectory $x^{(0)}(t)$. As a result, the expressions for the momentum $p_{st}$ and $S(t_f,t_s)$ are modified as follows [16]:

$$\begin{aligned} p_{st} = e[A(t_s)+ \\ \frac{\Delta B-A(t_s)\Delta t+\beta(0.5(\Delta B)^2-\Delta D+C(t_s)\Delta t)}{\Delta t-\beta(2\Delta G+\Delta t[B(t)+B(t_s)])}], \end{aligned} \quad (2)$$

$$\begin{aligned} S(t_f,t_s) &= S_0(t_f,t_s)+e^2\beta m_e^{-1}\{p(t_s)^2[2\Delta G \\ &+(B(t_f)+B(t_s))\Delta t]+p(t_s)[-\Delta C\Delta t \\ &+2\Delta D]+(C(t_f)+C(t_s))\Delta B-2\Delta F\}, \end{aligned} \quad (3)$$

where $\dot{D}(t)=C(t)$, $\dot{F}(t)=C(t)E(t)$, $\dot{G}(t)=B(t)$, $\beta=e/(m_e d_{inh})$. Another modification of the model is described by the function $H(t,t_s)$ under the integral in Eq. (2). This function is equal to 1 unless the electron hits during the motion the metal surface positioned at $d_{sur}$, otherwise we assume that the electron is absorbed by the surface and set $H(t,t_s)=0$.

#156477 - $15.00 USD Received 17 Oct 2011; revised 15 Nov 2011; accepted 15 Nov 2011; published 28 Nov 2011

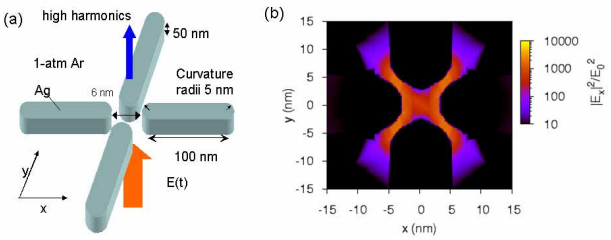


Fig. 1. Scheme (a) of polarization gating in HHG assisted by a crossed bowtie structure. The nanostructure is positioned on a silicon substrate and surrounded by Argon at 1 atm. The pump field is incident from below and normal to the surface. In (b), the intensity enhancement in the central part of the nanostructure at a vertical position of 25 nm is presented for a pump pulse centered at 800 nm.

To model the high harmonic generation in the vicinity of the metal nanostructure we first need to know the enhancement and spatial distribution of the electric field. For this aim we have utilized the commercial finite-element Maxwell solver JCMwave, which provides all components of the field as functions of the spatial coordinates for a monochromatic, linearly polarized input. The enhanced local field is calculated from the input field using this data for a set of wavelengths within the spectrum of the input pulse, including the depolarization (changing of the field direction) caused by the nanostructure. Note that different amplitudes and phases of the enhancement factors for different field components can lead to a change of the polarization state. In the case of a short-pulse excitation, the spatiotemporal profiles were reconstructed using the wavelength-dependent field redistribution and the spectral representation of the pump pulse. The phase change of the field due to the nanostructure was taken into account by using both amplitude and phase information provided by the JCMwave software. The obtained spatiotemporal field profiles were then substituted into the equations of the above-described model, to simulate high-harmonic output of the argon gas which surrounds the nanostructures. In these calculations, the temporal structure of the field as well as its time-dependent polarization state were fully taken into account, neither applying the approximations of a monochromatic pump pulse nor assuming near-cutoff emission by presuming zero starting velocity of electrons. In addition, for small curvature radii of the nanoparticle surface, the inhomogeneity of the field as well as collisions of the continuum-state electrons with the metal surface were taken into account.

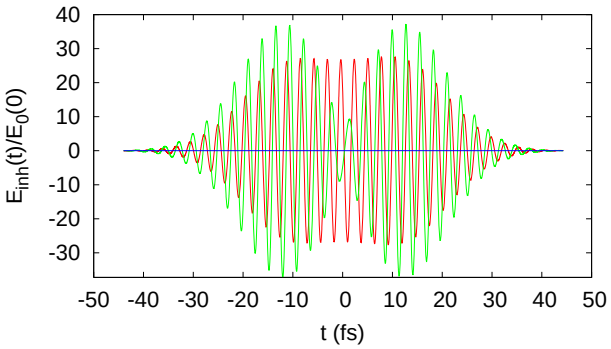


Fig. 2. Temporal dependence of the local electric fields in the ”hot spot” of the nanostructure shown in Fig. 1. The *x* (red curve) and the *y* (green curve) components of the field are normalized to the peak value of the incident field, the blue line denotes zero.

#156477 - $15.00 USD Received 17 Oct 2011; revised 15 Nov 2011; accepted 15 Nov 2011; published 28 Nov 2011

The boundary condition for the electric field normal to the surface causes an intensity reduction in silver by a factor of $1/|\varepsilon_{Ag}|^2 \sim 0.01$ to values below 5 TW/cm$^2$. Therefore we can assume that for the considered parameters the damage threshold of metal or metal nanostructures of about 0.1 J/cm$^2$ is not reached. For moderate laser intensities lower than 10 GW/cm$^2$ even and odd harmonics up to the fifth order can be generated from the metal surface but with an efficiency very rapidly decreasing with the harmonic order [19]. For higher intensities below relativistic values, no increase of the high-harmonic efficiency from metals was reported until the relativistic regime was reached, which implies that HHG in the gas will be the dominant source of harmonics for the application-relevant harmonic orders of above 10.

Unfortunately, a bowtie antenna [14] is not suitable for polarization gating of HHG. The reason is the difference in enhancement of fields which are polarized parallel and perpendicular to the bow-tie axis. The polarization of the local field does not necessarily follow the polarization of the incoming field. A circularly polarized pump pulse becomes almost linearly polarized in the local field, inhibiting the generation of single attosecond pulses. To circumvent this problem, we have designed the nanostructure shown in Fig. 1(a), which is characterized by the same values of the enhancement for both pump components in the "hot spots". A similar structure called cross-resonant optical antenna has been proposed earlier [20]. This nanostructure permits the translation of the polarization-gating shape of the pulse from the pump to the local fields. Note that in this case the lower radii of the curvature of the nanostructure and, in particular, the smaller gap between the nanostructure elements puts higher but not unrealistic requirements on the manufacturing technology. The distribution of the intensity enhancement (proportional to the square of the field) is shown in Fig. 1(b). A maximum enhancement of 1600 is achieved, with "hot spots" positioned symmetrically with respect to the $y = x$ and $y = -x$ lines. This assures that for both polarizations the enhancement values will be the same, and a circularly polarized incident beam will excite circularly polarized local fields in the "hot spots". Such a translation of the polarization state could fail outside of these hot spots; fortunately, only the hot spots are relevant for HHG.

To achieve polarization gating, the incident pulse must be shaped so that only a small portion of the pulse around its peak has linear polarization, while the remaining leading and trailing parts of the pulse are circularly polarized. Practically, this can be achieved by shaping the pulse, using e.g. half- and quarter-wavelength plates or a liquid-crystal spatial light modulator. We have simulated the input pulse by adopting some of the existing experimental approaches that are used in the polarization-gating experiments (e.g. [21]) and by propagating a 15-fs FWHM 830 nm Gaussian pulse through a 700-micron thick quartz plate followed by a zeroth-order $\lambda/4$ waveplate. The optical axis of the first plate is at 45 degrees with respect to the (initial) linear polarization while the second plate is turned 45 degrees with respect to the first. Next the one of the two orthogonal polarizations ($x$ and $y$) is attenuated as if the pulse would be passed through a plate at Brewster angle. Group velocity dispersion of the three plates is compensated. In Fig. 2, we show the temporal profile of the $x$ and $y$ components of the optimized pulse in the center of the "hot spot". Note how the almost-circular polarization at the leading edge goes over into a linear polarization near the center of the pulse, enabling efficient HHG only during a short time and leading to the generation of a single attosecond pulse. The wavelength-dependent phase contributions in the local fields, as well as the depolarization effects of the nanostructure do not have a strong influence on the shape of the pulse in the hot spot and on the generated harmonics.

In Fig. 3, the output high-harmonic spectrum (a) and the temporal shape (b) of the resulting single-attosecond pulse are shown for a pump intensity of 0.12 TW/cm$^2$. The spectrum presented in Fig. 3(a) shows a steady decline of the efficiency with harmonic number without a pronounced cutoff. This change in the spectral shape is caused by the field inhomogeneity and electron collisions with the metal surface, as explained in detail in Ref. [16]. Despite the some-

#156477 - $15.00 USD Received 17 Oct 2011; revised 15 Nov 2011; accepted 15 Nov 2011; published 28 Nov 2011

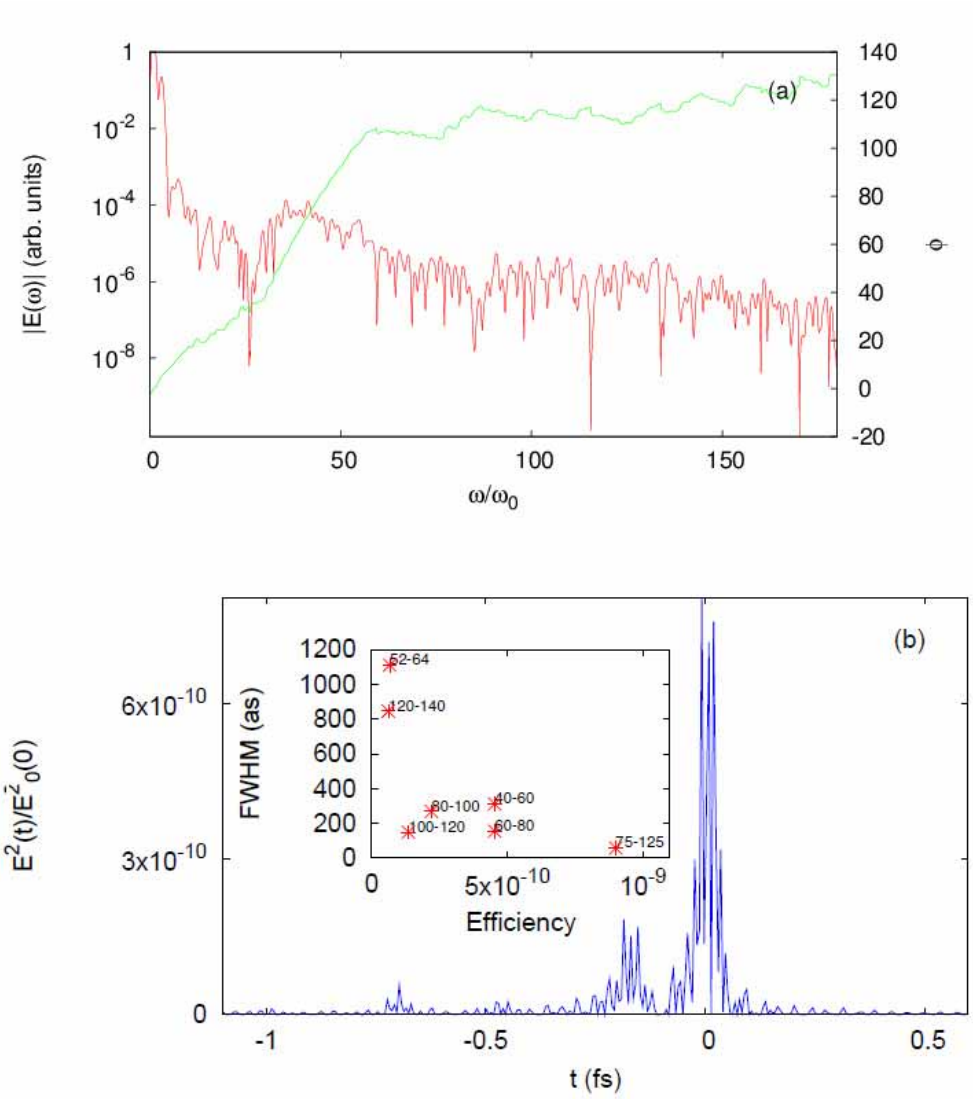


Fig. 3. Spectrum (a) and temporal profile (b) of the output attosecond pulse. The spectral components in the range below harmonic order 75 and above harmonic order 125 were filtered out to form an isolated attosecond pulse. The input peak intensity is 0.12 TW/cm$^2$. The inset indicates the durations and the efficiencies for other choices of harmonics forming the attosecond pulse, as indicated near the symbols. The green curve in (a) indicates the spectral phase.

what irregular nature of the spectrum in Fig. 3(a), a single attosecond pulse can be obtained from it. We predict that this can be achieved by filtering out harmonics with numbers below 75 and above 125. The remaining portion of the spectrum, which correspond to photons in the energy range from 112 to 187 eV, forms a single, 59-attosecond pulse with a temporal shape shown in Fig. 3(b). This pulse is characterized by a low pedestal, with a small satellite pulse on the leading edge. Additionally, we have repeated the calculations excluding the effect of distortions caused by the wavelength-dependent phase of the local fields as well as the polar-

#156477 - $15.00 USD Received 17 Oct 2011; revised 15 Nov 2011; accepted 15 Nov 2011; published 28 Nov 2011

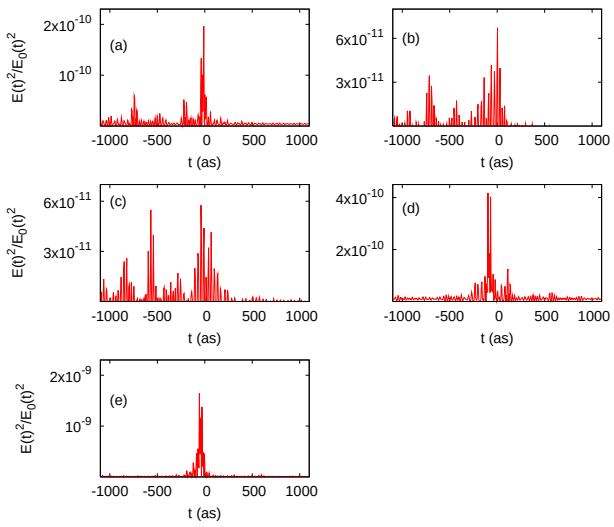


Fig. 4. Attosecond pulses generated with carrier-envelope offset of $18^o$ (a), $36^o$ (b), $54^o$ (c), $72^o$ (d), and $90^o$ (e). The parameters are the same as in the case shown in Fig. 3(a).

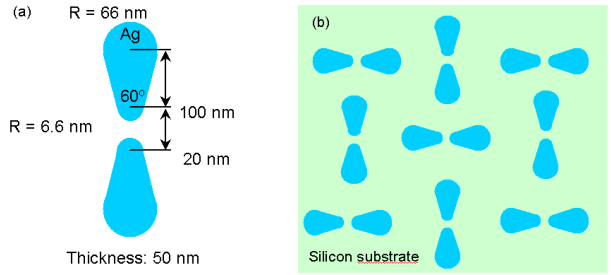


Fig. 5. Geometry of the nanostructures and their arrangement for circular-polarization HHG. We assume a silicon substrate and 1-atm Argon surrounding the nanostructure. The circularly polarized pump light irradiates the structure under normal incidence from below.

ization change induced by the nanostructure. In this case, the FWHM duration of the pulse is 64 attosecond, indicating that these nanoparticle-related effects do not play a dominant role. The efficiency of the conversion is roughly $10^{-9}$, assuming that the nanostructures are densely distributed over the substrate. In addition, in the inset of Fig. 3(b) the durations and the efficiencies for other choices of harmonics are shown, indicating that the attosecond pulse is longer and/or weaker than the one shown in Fig. 3(b) for the choice of harmonic numbers from 75 to 125. Thus we can conclude that HHG in the vicinity of the nanostructure can be used in combination with the polarization gating technique, leading to the generation of single attosecond pulses with a FWHM of about 100 attoseconds.

The dependence of the generated attosecond pulse on the carrier-envelope offset of the pump is an important issue in practical stuations. We adress this issue in Fig. 4, where the generated pulses are shown for several carrier-envelope offsets. One can see that for the carrier-envelope offsets around $45^o$ the pulse becomes longer and irregular, while at $90^o$ offset we again obtain an isolated attosecond pulse. This result for a carrier-evenlope offset of 90 degrees [Fig. 4(e)] is even superior to the result obtained for an offset of 0 degrees, since in this case the 57-attosecond pulse is formed without a pre-pulse. The origin of the strong dependence of the

#156477 - $15.00 USD Received 17 Oct 2011; revised 15 Nov 2011; accepted 15 Nov 2011; published 28 Nov 2011

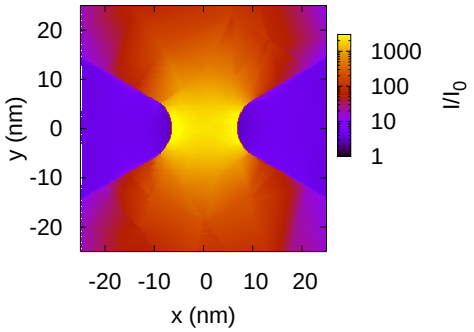


Fig. 6. Field enhancement in the center of the nanostructure at the vertical position of 25 nm for a continuous-wave pump at 800 nm.

generated pulse on the carrier-envelope offset lies in the small duration of the time when the polarization is almost linear, so that the electric field value at this time influences the electron trajectories and the emitted high harmonics.

Next we will investigate the possibilities to generate circularly polarized HHG, which is forbidden in traditional HHG, by exploiting the polarization properties of single bowtie antennae. We have considered the ensemble of nanostructures depicted in Fig. 5(b). The ensemble consists of equal numbers of vertically and horizontally oriented bowtie-type nanoantennae on a silicon substrate. A single nanoantenna and its geometrical parameters are shown separately in Fig. 5(a). We note that the curvature radii, the separation between the elements, and the nanoantenna thicknesses indicated in the caption of Fig. 5 are within reach of modern lithographic technology. The circularly polarized pump light is incident from the bottom of the structure and can be represented by the sum of the *x*-polarized and *y*-polarized components, with a $\pi/2$ phase offset. Each of the components of the pump light is strongly enhanced by the bowtie nanoattennae parallel to its electric field. This enhancement is illustrated in Fig. 6, where the distribution of the squared *x* component of the local field over space is given for a *x*-polarized pump pulse. The maximum achievable intensity enhancement is around 1000, while for the *y*-polarized pump the value of the *x* component of the local-field enhancement is below 1 in the gap between the elements of the nanoantenna.

This contrast between the local field enhancements of the *x*- and *y*-polarized pump components can be utilized for the generation of circularly-polarized harmonics by using a circularly-polarized pump. Each of the components is highly enhanced in the gap of half of the nanoantennas for which the axis is parallel to the polarization vector. The local field in the nanoantennas normal to this field component is barely influenced. Therefore the field in the vicinity of each element is (almost) linearly polarized, permitting high harmonic generation with high efficiency, not hindered by the circular polarization. Since the phase offset between the harmonic components is the phase offset between the pump components multiplied by the harmonic number, the output radiation will form a circularly polarized harmonic beam in the far field of the nanoelement array. Note that the rotation direction of the $4N+1$th (fifth, ninth, etc.) harmonics will coincide with that of the pump, while the $4N+3$th (third, seventh, etc.) harmonics will also be circularly polarized but rotate in the opposite direction. From this it follows that these harmonics would be a suitable source for circular dichroism measurements, where the handedness of the incident circular polarization controls the handedness of the harmonics generated.

#156477 - $15.00 USD Received 17 Oct 2011; revised 15 Nov 2011; accepted 15 Nov 2011; published 28 Nov 2011

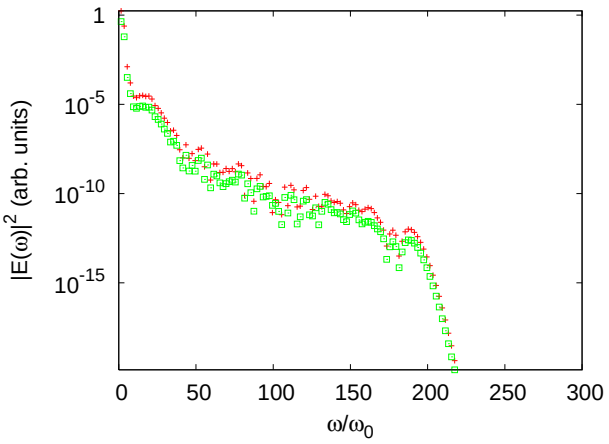


Fig. 7. Spectra of the emitted circularly-polarized harmonics (red crosses) with circularly-polarized pump and of the linearly-polarized harmonics (green squares) using linearly polarized pump pulses with the same peak electric field value. The incident pump intensity is 0.3 TW/cm$^2$.

In Fig. 7, the output spectrum of the emitted circularly-polarized harmonics is shown by the red crosses for a 0.3-TW/cm$^2$ continuous-wave pump at 800 nm for 1 atm argon pressure surrounding the nanoantennae. One can see a typical plateau-and-cutoff behavior which is characteristic for a linearly polarized pump. The conversion efficiency is about $10^{-10}$ in the middle of the plateau. We conclude that this arrangement of nanoantennae can be used for an efficient circular-polarization HHG. The high-harmonic dipole moment of such nanoparticle ensemble leads to the emission of circularly polarized harmonics within a narrow emission angle which depends on the ensemble size. Note that the radiation emitted at larger angles could have other polarization properties. In Fig. 7 the conversion efficiency for the linearly-polarized pump is shown for comparison by the green squares, showing values lower by a factor of roughly 4.

## Conclusion

In conclusion, we studied plasmon-enhanced high-order harmonic generation in the vicinity of specifically designed nanostructures enabling the application of the HHG polarization gating technique. Besides field enhancement such structures permit the generation of isolated attosecond pulses by longer, low-intensity pump pulses; in a considered example the generation of isolated 59-attosecond pulses from 15-fs, 0.6 TW/cm$^2$ pump pulses has been predicted. Additionally, we studied the possibility to generate high harmonics with circular polarization which is impossible in the traditional generation method. We predict that arrays consisting of equal numbers of mutually normally-oriented nanostructures allow the generation of circularly polarized harmonics from circularly polarized pump pulses, which can be used for circular dichroism measurements. The results are obtained using a finite-element method for the calculation of the field enhancement and an extended Lewenstein model which includes the field inhomogeneity in the hot spots and the possible collisions of the electrons with the metal surface.

#156477 - $15.00 USD Received 17 Oct 2011; revised 15 Nov 2011; accepted 15 Nov 2011; published 28 Nov 2011